Electron radiated power in cyclotron radiation emission spectroscopy experiments

A. Ashtari Esfahani,[1,*] V. Bansal,[2] S. Böser,[3] N. Buzinsky,[4] R. Cervantes,[1] C. Claessens,[3] L. de Viveiros,[5] P. J. Doe,[1] M. Fertl,[1] J. A. Formaggio,[4] L. Gladstone,[6] M. Guigue,[2,†] K. M. Heeger,[7] J. Johnston,[4] A. M. Jones,[2] K. Kazkaz,[8] B. H. LaRoque,[2] M. Leber,[9] A. Lindman,[3] E. Machado,[1] B. Monreal,[6] E. C. Morrison,[2] J. A. Nikkel,[7] E. Novitski,[1] N. S. Oblath,[2] W. Pettus,[1] R. G. H. Robertson,[1] G. Rybka,[1,‡] L. Saldaña,[7] V. Sibille,[4] M. Schram,[2] P. L. Slocum,[7] Y.-H. Sun,[6] J. R. Tedeschi,[2] T. Thümmler,[10] B. A. VanDevender,[2] M. Wachtendonk,[1] M. Walter,[10] T. E. Weiss,[4] T. Wendler,[5] and E. Zayas[4]
(Project 8 Collaboration)

[1]*Center for Experimental Nuclear Physics and Astrophysics and Department of Physics, University of Washington, Seattle, Washington 98195, USA*
[2]*Pacific Northwest National Laboratory, Richland, Washington 99354, USA*
[3]*Institut für Physik, Johannes Gutenberg-Universität Mainz, 55128 Mainz, Germany*
[4]*Laboratory for Nuclear Science, Massachusetts Institute of Technology, Cambridge, Massachusetts 02139, USA*
[5]*Department of Physics, Pennsylvania State University, State College, Pennsylvania 16801, USA*
[6]*Department of Physics, Case Western Reserve University, Cleveland, Ohio 44106, USA*
[7]*Wright Laboratory, Department of Physics, Yale University, New Haven, Connecticut 06520, USA*
[8]*Lawrence Livermore National Laboratory, Livermore, California 94550, USA*
[9]*Department of Physics, University of California Santa Barbara, California 93106, USA*
[10]*Institut für Kernphysik, Karlsruher Institut für Technologie, 76021 Karlsruhe, Germany*

(Received 10 January 2019; published 2 May 2019)

The recently developed technique of Cyclotron Radiation Emission Spectroscopy (CRES) uses frequency information from the cyclotron motion of an electron in a magnetic bottle to infer its kinetic energy. Here we derive the expected radio-frequency signal from an electron in a waveguide CRES apparatus from first principles. We demonstrate that the frequency-domain signal is rich in information about the electron's kinematic parameters and extract a set of measurables that in a suitably designed system are sufficient for disentangling the electron's kinetic energy from the rest of its kinematic features. This lays the groundwork for high-resolution energy measurements in future CRES experiments, such as the Project 8 neutrino mass measurement.

DOI: 10.1103/PhysRevC.99.055501

I. INTRODUCTION TO CYCLOTRON RADIATION EMISSION SPECTROSCOPY

Following the invention of the Penning trap [1], low-energy electrons bound with electric and magnetic fields have been used to make some of the most precise measurements of fundamental physics values (e.g., the $g-2$ of the electron [2,3]). The success of these measurements was contingent on a well-developed theory relating the signal from the axial motion of the electron in the trap to the electron's kinematic parameters [4].

Recently it has been proposed [5] that the technique called Cyclotron Radiation Emission Spectroscopy (CRES) [6] may be used to make precision measurement of nuclear β decay. In CRES, decay electrons or positrons are trapped in a magnetic bottle, and the cyclotron radiation from these particles gives direct information about their total energy. Since an electric field would introduce a position-dependent component to the particle energy, studies of radioactive decay require a purely magnetic trap, eliminating the possibility of a full Penning trap configuration.

At present, the primary application of CRES being investigated is an endpoint measurement of tritium for the purposes of measuring the neutrino mass scale by the Project 8 collaboration [6,7]. The determination of the neutrino mass via a tritium endpoint measurement is a well-studied process [8], but successful execution requires exquisite electron energy measurement, high rejection of low-energy electron signals, and a deep understanding of systematic uncertainties in both electron energy and detection efficiency. CRES is also being explored to improve measurement of Fierz interference in neutron and nuclear β decay, which is currently limited by detector systematics [9,10].

In order to address the understanding of systematic uncertainties in Project 8 and other nuclear physics experiments dependent on CRES, we develop here a mathematical description that relates the characteristics of the apparatus, the motion of the electron, and the measured signal.

For the purposes of this paper, we will consider the current configuration of the Project 8 prototype experiment where electrons are produced and trapped inside a waveguide. The

*ashtari@uw.edu
†Now at Sorbonne Université and Laboratoire de Physique Nucléaire et des Hautes Énergies, CNRS/IN2P3, 75005 Paris, France; mguigue@lpnhe.in2p3.fr
‡grybka@uw.edu

waveguide propagates the cyclotron radiation emitted by the electrons to a receiver with minimal losses. The background magnetic field within the waveguide consists of two contributions: a strong, uniform, background field, which is parallel to the axis of the waveguide, and a magnetic distortion which forms the magnetic bottle.

In Sec. II, we investigate the variation of the cyclotron frequency due to the electron's motion. In Sec. III, we derive the electron's radiation spectrum into the waveguide. In Sec. IV, we study the effects of signal reflections on the measured radiation spectrum. In Sec. V, we apply the formulas from Secs. II, III, and IV to two examples of magnetic bottle configurations. Finally, in Secs. VI and VII, we demonstrate that there is sufficient information in the signal to reconstruct the kinematic parameters of the electron.

II. MOTION AND CYCLOTRON FREQUENCY OF AN ELECTRON IN A MAGNETIC BOTTLE

A. The need for a magnetic trap

The angular cyclotron frequency, Ω_c, of an electron with kinetic energy K_e and mass m_e, in a magnetic field B, is given by

$$\Omega_c = \frac{eB}{\gamma m_e} = \frac{eB}{m_e + K_e/c^2}, \tag{1}$$

where e is the elementary charge, c is the speed of light, and γ the electron's Lorentz factor. For a known magnetic field, a measurement of the frequency of an electron's cyclotron radiation is also a determination of its kinetic energy [6]. The frequency resolution of the measurement, and therefore the energy resolution, improves with increasing observation time. Therefore a no-work trap is necessary for an electron to be observed for a sufficiently long time.

B. Magnetic bottle and pitch-angle definition

A magnetic bottle consists of a local minimum in the magnitude of background magnetic field. The behavior of a charged particle in a magnetic bottle has been well described [4,11], so here we highlight only the elements important for our results. If we define an electron's instantaneous pitch angle, $\theta(t)$, as the angle between the local magnetic field and the electron's momentum, then the kinetic energy for an electron undergoing cyclotron motion can be decomposed to its parallel and perpendicular components as

$$\begin{aligned} K_e &= K_{e\parallel} + K_{e\perp} \\ &= \frac{1}{2}\frac{p_0^2}{m_e}\cos^2\theta(t) + \mu(t)B(t), \end{aligned} \tag{2}$$

where p_0 is the magnitude of the electron's initial momentum and μ is the equivalent magnetic moment of the electron, given by

$$\mu(t) = \frac{1}{2}\frac{p_0^2}{m_e}\frac{\sin^2\theta(t)}{B(t)}. \tag{3}$$

In the adiabatic regime, where the change in the magnetic field direction is slow compared with the cyclotron frequency, an electron's equivalent magnetic moment is a constant of motion. For the remainder of this derivation μ is treated as time independent and the term $\mu B(t)$ behaves as a magnetic potential energy. Electrons with pitch angles of $90 + \delta\theta^\circ$ or $90 - \delta\theta^\circ$ will have the same motion; therefore we will only consider electrons with pitch angles between 0 and 90°. The pitch angle approaches 90° for an electron exploring regions of increasing magnetic field, whereas the pitch angle decreases for an electron approaching the bottom of the trap. For every electron, we define the pitch angle at the bottom of the trap to be θ_{bot}. Due to conservation of energy, the condition on pitch angle for a trapped electron is

$$\theta_{\text{bot}} \geqslant \sin^{-1}\left(\sqrt{1 - \frac{\Delta B}{B_{\text{max}}}}\right), \tag{4}$$

where B_{max} is the maximum value of the magnetic field and ΔB is the trap depth.

Existing CRES experiments operate at a background field of 1T, which we use for all examples throughout. A 4mT trap depth on this background field can trap electrons with pitch angles greater than 86°. As a consequence, electrons trapped in the magnetic bottle with a pitch angle other than 90° at the bottom of the trap will undergo periodic axial motion as depicted in Fig. 1.

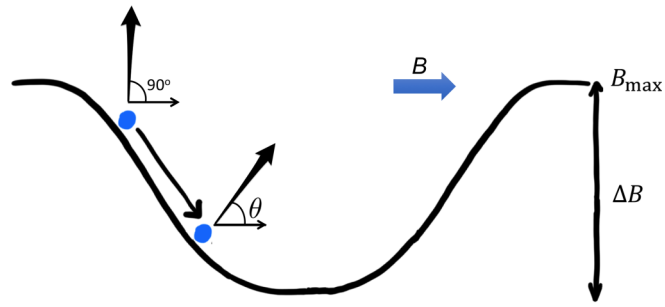

FIG. 1. Axial motion of an electron in a magnetic bottle. The magnetic trap has depth ΔB and maximum value B_{max}. The electron's pitch angle is defined as the angle between the electron's momentum vector and the direction of the local magnetic field. If the electron's pitch angle at the bottom of the trap satisfies Eq. (4), then the electron undergoes an oscillatory axial motion inside the trap. The turning point for the electron corresponds to the position when the pitch angle is 90°.

C. Time-varying cyclotron frequency of an electron

The magnetic field experienced by an electron varies with time due to its axial motion, resulting in a time-varying cyclotron frequency, given by

$$\Omega_c(t) = \frac{eB(t)}{m_e + K_e/c^2}. \tag{5}$$

Additionally, the electron's cyclotron motion causes it to radiate, reducing its kinetic energy and therefore increasing its cyclotron frequency. This energy loss can be expressed as

$$\frac{dK_e(t)}{dt} = -P(t), \tag{6}$$

where P, the power radiated by the electron, can be assumed to be constant over short times. The energy radiated is much smaller than the electron's initial total energy. Therefore, the instantaneous frequency of radiation emitted by the electron can be derived from Eq. (1) as

$$\Omega_c(t) \simeq \frac{eB(t)}{m_e + K_0/c^2}\left(1 + \frac{Pt}{m_e c^2 + K_0}\right), \tag{7}$$

where K_0 is the initial kinetic energy of the electron. Because the cyclotron radiation is observed for a finite amount of time, the frequency is shifting by the electron power loss $\frac{Pt}{m_e c^2 + K_0}$.

Existing CRES experiments operate with mildly relativistic electrons, we take a 30-keV electron for examples throughout. Such an electron in a 1-T background field radiates 1 fW of power. Over 10 μs this results in a cyclotron frequency shift of 3 kHz, which is equivalent to an energy shift of 60 meV. This effect can be ignored in the following calculation of CRES power spectral density. We will consider it again when we introduce the slope of tracks in Sec. VI.

D. Axial motion and Doppler shift

As a trapped electron oscillates axially in a magnetic bottle, the frequency of radiation collected by the receiver on the same axis, Ω_r, is shifted by the Doppler effect and can be expressed as

$$\Omega_r(t) = \Omega_c(t_{\rm ret})\left[1 - \frac{v_z(t_{\rm ret})}{v_p}\right]^{-1}, \tag{8}$$

where $t_{\rm ret}$ is the retarded time, v_z is the electron axial velocity, and v_p is the phase velocity of the wave inside the waveguide. For mildly relativistic electrons with the large pitch angles required for trapping, the term $\frac{v_z(t_{\rm ret})}{v_p}$ is small compared to 1. Substituting Ω_c from Eq. (7) into Eq. (5) results in

$$\Omega_r(t) \simeq \frac{eB(t_{\rm ret})}{m_e + K_0/c^2}\left[1 + \frac{v_z(t_{\rm ret})}{v_p}\right], \tag{9}$$

in which the second-order contributions in v_z/v_p have been neglected. Equation (9) introduces two systematic effects that must be accounted for to understand the relationship between the electron's energy and the observed signal.

First, the average value of $B(t)$ is greater than the value of B at the center of the trap and depends on the magnitude of the electron's axial motion. This causes the average measured frequency to be dependent on the electron's motion in the trap. This feature has been briefly discussed in Ref. [6], for electrons in a harmonic trap, and will be discussed in detail in Sec. V.

Second, the terms $B(t)$ and $v_z(t)$ vary periodically at harmonics of the frequency of the electron's axial motion. This imposes frequency modulation on the cyclotron signal, both by the varying magnetic field and by the Doppler shift, with the modulation due to the magnetic field being the smaller of the two effects. Frequency-modulated signals have been studied extensively as a form of encoding information in radio-frequency signals [12]. The expected signal at the receiver consists of a frequency comb structure, where the main carrier is at the average cyclotron frequency and is surrounded by sidebands which are evenly spaced by the frequency of axial motion as shown in Fig. 2.

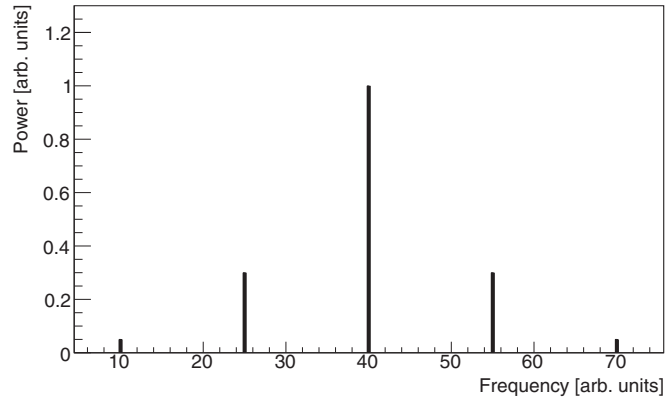

FIG. 2. The comb structure of the frequency spectrum of cyclotron power from a trapped 30-keV electron in a 1-T background field. The central peak is located at the average cyclotron frequency, and the axial frequency, which defines the separation between the peaks, is 15 MHz.

The relative magnitude of the sidebands can be characterized by the modulation index, $h = \frac{\Delta\omega}{\omega_a}$, where $\Delta\omega$ is the maximum frequency change due to the Doppler shift and magnetic field and ω_a is the axial frequency. The magnitude of the nth sideband is given by the Bessel function $J_n(h)$. For values of h greater than 0.5, a significant fraction of power is present in the sidebands. For $h \simeq 2.41$, all of the power is radiated in sidebands, and no power is radiated into the carrier, as shown in Fig. 5.

As a simple case, we can calculate the sideband structure from only the Doppler shift for an electron moving axially in simple harmonic motion, with axial frequency ω_a and maximum travel $z_{\rm max}$. From Eq. (9) we note that the maximum frequency change is $\Delta\omega = \Omega_c \omega_a z_{\rm max}/v_p$. The modulation index is then $h = \frac{\Omega_c z_{\rm max}}{v_p}$. The threshold for significant received signal power in the sidebands, $h \sim 0.5$, is therefore equivalent to an axial travel for electrons greater than a half-wavelength of light in waveguide.

E. Grad-B and curvature drifts

The electron undergoes a cyclotron motion, an axial motion, and two drift motions induced by nonuniformity in the magnetic field. The first force is prompted by the magnetic gradient in the trap. These local magnetic field gradients exert a force on the electron that gives rise to a drift velocity perpendicular to both the magnetic field and its gradient, which we call grad-B motion, given by [13]

$$\mathbf{v}_{\rm grad-B} = \frac{\mu}{m\Omega_c B}\mathbf{B} \times \nabla B. \tag{10}$$

This slow grad-B motion is analogous in its effect to magnetron motion in a Penning trap; it pins the guiding center of the electron's cyclotron motion to a larger circle. The radius of this larger circle is set by the electron's radial position in the trap at the moment it is created.

The grad-B velocity for a 30-keV electron with pitch angle of 86° in a 1-T magnetic field with a 10-mT/m field gradient is smaller than 300 m/s. This velocity corresponds to a frequency of 5 kHz for an electron orbit with a 1cm radius. For power spectral densities calculated for a finite time length smaller than grad-B motion's period, this effect can be ignored and the electron's guiding center can be assumed fixed.

The curvature in the field lines introduces another drift motion, which we call curvature drift, given by [13]

$$\mathbf{v}_{\text{curv}} = \frac{v_0^2 \cos^2[\theta(t)]}{\Omega_c B^3} \mathbf{B} \times (\mathbf{B} \cdot \nabla)\mathbf{B}. \tag{11}$$

For the conditions described below Eq. (10), the curvature drift is smaller than 3 m/s and therefore negligible. For a detailed study of these two effects look at Refs. [14] and [15].

III. RADIATION OF A TRAPPED ELECTRON INTO A WAVEGUIDE MODE

We now derive generic expressions for the spectral distribution of the cyclotron radiation of a trapped electron. We first expand the radiation from a generic current inside the waveguide volume in terms of waveguide modes and derive the power that propagates through the waveguide. We then discuss the specific case of an electron coupling to a waveguide and the associated approximations (as done with more detail in Ref. [16]). This allows us to show that the mode excitation can be written in term of harmonics, corresponding to the axial modes, which demonstrates the comb structure of the measured cyclotron power. Finally, we discuss the implications of our results in two examples, rectangular and circular waveguides.

A. Waveguide modes and transmitted power

Generalizing the notation in Jackson [15], the electric and magnetic fields inside a waveguide can be written as a sum over all modes in the $\pm z$ directions as

$$\begin{aligned}\mathbf{E}^{\pm}(\mathbf{r},t) &= \sum_{\lambda} \int_{-\infty}^{\infty} A_{\lambda}^{\pm}(\omega)[\mathbf{E}_{t\lambda}(x,y) \pm E_{z\lambda}(x,y)\hat{\mathbf{z}}] \\ &\quad \times e^{\pm ik_{\lambda}z} e^{-i\omega t} d\omega \\ \mathbf{H}^{\pm}(\mathbf{r},t) &= \sum_{\lambda} \int_{-\infty}^{\infty} A_{\lambda}^{\pm}(\omega)\left[\pm\frac{1}{Z_{\lambda}}\hat{\mathbf{z}} \times \mathbf{E}_{t\lambda}(x,y) + H_{z\lambda}(x,y)\hat{\mathbf{z}}\right] \\ &\quad \times e^{\pm ik_{\lambda}z} e^{-i\omega t} d\omega, \end{aligned} \tag{12}$$

where k_λ is the wave number and Z_λ the mode impedance. The amplitude, $A_\lambda(\omega)$, of each mode is found via Poynting's theorem and is given by

$$A_{\lambda}^{\pm}(\omega) = -\frac{Z_{\lambda}}{2} \int_V \mathbf{J}(\omega) \cdot [\mathbf{E}_{t\lambda}(x,y) \mp E_{z\lambda}(x,y)\hat{\mathbf{z}}] e^{\mp ik_{\lambda}z} d^3r, \tag{13}$$

with V being the waveguide volume and the current inside the waveguide, $\mathbf{J}(\omega)$, defined as

$$\mathbf{J}(\omega) = \frac{1}{2\pi} \int_{-\infty}^{\infty} \mathbf{J}(\mathbf{r},t) e^{i\omega t} dt. \tag{14}$$

These mode amplitudes fully determine the signal in the waveguide. The transverse electric field modes, $\mathbf{E}_{t\lambda}(x,y)$, are normalized over the waveguide cross section $\mathcal{A}$ such that

$$\int_{\mathcal{A}} \mathbf{E}_{t\lambda} \cdot \mathbf{E}_{t\mu} da = \delta_{\lambda\mu}. \tag{15}$$

The longitudinal electric field modes, $\mathbf{E}_{z\lambda}(x,y)$, are normalized for TM modes such that

$$\int_{\mathcal{A}} E_{z\lambda} E_{z\mu} da = -\frac{\gamma_{\lambda}^2}{k_{\lambda}^2} \delta_{\lambda\mu}, \tag{16}$$

with γ_λ being the mode eigenvalues, which are zero for TE modes.

The power transmitted in the $\pm z$ direction is a spatial integral of the normal component of the Poynting vector, taken over the waveguide's cross section, $\mathcal{A}$. It can be written as

$$\begin{aligned} P^{\pm}(t) &= \int_{\mathcal{A}} \mathbf{E}^{\pm}(\mathbf{r},t) \times \mathbf{H}^{\pm}(\mathbf{r},t) \cdot (\pm\hat{\mathbf{z}})\, da \\ &= \sum_{\lambda} \frac{1}{Z_{\lambda}} [B_{\lambda}^{\pm}(t)]^2, \end{aligned} \tag{17}$$

in which the mode excitation, $B_\lambda^{\pm}(t)$, not to be confused with the B-field, is defined as

$$B_{\lambda}^{\pm}(t) = \int_{-\infty}^{\infty} A_{\lambda}^{\pm}(\omega) e^{\pm ik_{\lambda}z} e^{-i\omega t} d\omega. \tag{18}$$

B. Power spectral density

Power spectral density is the quantity which we ultimately aim to calculate. To that end, we define the power spectral density of the mode excitation as

$$\tilde{P}^{\pm}(\omega) = \frac{2\pi}{T} \sum_{\lambda} \frac{1}{Z_{\lambda}} |\tilde{B}_{\lambda}^{\pm}(\omega)|^2, \tag{19}$$

with

$$\tilde{B}_{\lambda}^{\pm}(\omega) = \frac{1}{2\pi} \int_{-\infty}^{+\infty} B_{\lambda}^{\pm}(t) e^{i\omega t} dt = A_{\lambda}^{\pm}(\omega) e^{\pm ik_{\lambda}z}, \tag{20}$$

and T being the total time of observation. Equation (19) can be interpreted as the sum of the power in each waveguide mode,

$$\tilde{P}^{\pm}(\omega) = \sum_{\lambda} \tilde{P}_{\lambda}^{\pm}(\omega), \tag{21}$$

where

$$\tilde{P}_{\lambda}^{\pm}(\omega) = \frac{2\pi}{T} \frac{1}{Z_{\lambda}} |\tilde{B}_{\lambda}^{\pm}(\omega)|^2. \tag{22}$$

In the case of a single electron, moving on the trajectory $\mathbf{r} = \mathbf{r}_0(t)$ with the velocity $\mathbf{v}(t)$, the current density is

$$\mathbf{J}(\mathbf{r},t) = -e\mathbf{v}(t)\delta^3[\mathbf{r} - \mathbf{r}_0(t)]. \tag{23}$$

From this and Eq. (13), the mode amplitudes can be found to be

$$\begin{aligned} A_{\lambda}^{\pm}(\omega) = &-\frac{Z_{\lambda}}{4\pi} \int_V \int_{-\infty}^{\infty} e\mathbf{v}(t) \cdot [\mathbf{E}_{t\lambda}(x,y) \mp E_{z\lambda}(x,y)\hat{\mathbf{z}}] \\ &\times \delta^3[\mathbf{r} - \mathbf{r}_0(t)] e^{i\omega t} e^{\mp ik_{\lambda}z} dt d^3r. \end{aligned} \tag{24}$$

By changing the order of integrals and taking the spatial integral, we find that

$$A_\lambda^\pm(\omega) = -\frac{eZ_\lambda}{4\pi}\int_{-\infty}^{\infty}\mathbf{v}(t)\cdot[\mathbf{E}_{t\lambda}(x_0(t),y_0(t)) \mp E_{z\lambda}(x_0(t),y_0(t))\hat{\mathbf{z}}]e^{i\omega t}e^{\mp ik_\lambda z_0(t)}dt, \quad (25)$$

where the field is evaluated at the electron's position, $\mathbf{r}_0(t) = (x_0(t), y_0(t), z_0(t))$. Using the mode amplitudes, the procedure from the preceding section is used to find $\tilde{B}_\lambda^\pm(\omega)$, from which the energy losses and signal power follow.

C. Field amplitudes for a CRES electron

Equation (25) describes the coupling of an electron inside a waveguide, without any assumptions about its motion. A number of reasonable approximations can be used in the case of an electron in a CRES experiment.

The electron's periodic motion can be decomposed into a cyclotron motion, an axial motion, and a drift motion. Following the discussion of Sec. II E we assume this last motion is slow compared with the first two, so the electron's transverse and longitudinal velocity components can be written as

$$\begin{aligned}\mathbf{v}_t(t) &= v_0\sin\theta(t)[\cos\Phi_c(t)\mathbf{e}_1 + \sin\Phi_c(t)\mathbf{e}_2]\\ v_z(t) &= v_0\cos\theta(t),\end{aligned} \quad (26)$$

where $(\mathbf{e}_1, \mathbf{e}_2)$ is an orthonormal basis in the plane transverse to the z direction, v_0 is the electron's initial velocity, and $\Phi_c(t)$ is the phase of the electron in its cyclotron orbit, defined as

$$\Phi_c(t) = \int_0^t \Omega_c(t')dt'. \quad (27)$$

This phase can also be written as a combination of constant phase progression at the average cyclotron frequency, Ω_0, and a periodic perturbation at the electron's axial frequency.

The $\mathbf{v}\cdot\mathbf{E}$ term in Eq. (25), at the position $(x_0(t), y_0(t))$, can then be written as

$$\mathbf{v}(t)\cdot(\mathbf{E}_{t\lambda} \mp E_{z\lambda}\hat{\mathbf{z}}) = v_0\sin\theta(t)\{E_{1\lambda}\cos[\Phi_c(t)] + E_{2\lambda}\sin[\Phi_c(t)]\} \mp \cos\theta(t)E_{z\lambda}), \quad (28)$$

where $E_{1\lambda}$ and $E_{2\lambda}$ are the components of the transverse electric field for the mode λ.

The radius of the cyclotron motion, r_c, and the wavelength of the cyclotron radiation, λ_c, are related via

$$r_c = \frac{v}{2\pi c}\lambda_c. \quad (29)$$

As a result, the radius of cyclotron motion is small compared to the wavelength of cyclotron radiation and therefore the waveguide dimensions. The variation in coupling due to the cyclotron motion can be neglected, and one can replace the actual position of the electron by its gyrocenter, defined to be the center of the electron's cyclotron motion. In this work, we will further assume the transverse position of the electron's gyrocenter (x_c, y_c) does not change with time. This may not be true in experiments with significant drift motion.

The z component of the $\mathbf{v}\cdot\mathbf{E}$ term in Eq. (25) is equal to zero for transverse electric (TE) modes and small in transverse magnetic (TM) modes for electrons with large pitch angles. The phase oscillation induced by $\sin\theta(t)$ in Eq. (28) is thus small compared with the cyclotron phase Φ_c and can be neglected.

Using the above approximations, Eq. (28) can be rewritten as

$$\begin{aligned}\mathbf{v}\cdot\mathbf{E} &= v_0\{E_{1\lambda}(x,y)\cos[\Phi_c(t)] + E_{2\lambda}(x,y)\sin[\Phi_c(t)]\}\\ &= \frac{v_0}{2}[(E_{1\lambda} - iE_{2\lambda})e^{i\Phi_c(t)} + (E_{1\lambda} + iE_{2\lambda})e^{-i\Phi_c(t)}].\end{aligned} \quad (30)$$

Replacing the above expression for $\mathbf{v}\cdot\mathbf{E}$ in Eq. (25) we get

$$A_\lambda^\pm(\omega) = -\frac{eZ_\lambda v_0}{8\pi}\left[(E_{1\lambda} - iE_{2\lambda})\int_{-\infty}^{\infty}e^{i\Phi_c(t)}e^{\mp ik_\lambda z_0(t)}e^{i\omega t}dt + (E_{1\lambda} + iE_{2\lambda})\int_{-\infty}^{\infty}e^{-i\Phi_c(t)}e^{\mp ik_\lambda z_0(t)}e^{i\omega t}dt\right], \quad (31)$$

where the electric fields are being evaluated at the electron's gyrocenter (x_c, y_c).

D. Mode expansion of motion and phase

Because $z_0(t)$ and $\Phi_c(t) - \Omega_0 t$ are periodic at the electron's axial motion frequency Ω_a, these terms can be expanded in a Fourier series as

$$e^{i\Phi_c(t) - i\Omega_0 t} = \sum_{m=-\infty}^{\infty}\alpha_m e^{im\Omega_a t} \quad (32)$$

and

$$e^{ik_\lambda z(t)} = \sum_{m=-\infty}^{\infty}\beta_m(k_\lambda)e^{im\Omega_a t}. \quad (33)$$

As a result, the exponential term in Eq. (31) can be written as

$$e^{i\Phi_c(t) + ik_\lambda z_0(t)} = \sum_{n=-\infty}^{\infty}a_n(k_\lambda)e^{i(\Omega_0 + n\Omega_a)t}, \quad (34)$$

in which

$$a_n(k_\lambda) = \sum_{m=-\infty}^{\infty}\alpha_m(k_\lambda)\beta_{n-m}(k_\lambda). \quad (35)$$

These coefficients, a_n, can be computed from a decomposition of the axial motion and the cyclotron phase evolution into harmonics of the axial frequency. This greatly simplifies the study of the radiated power spectral density.

Based on Eq. (35), we get the following:

$$\begin{aligned}e^{i\Phi_c(t) - ik_\lambda z_0(t)} &= \sum_{n=-\infty}^{\infty}a_n(-k_\lambda)e^{i(\Omega_0 + n\Omega_a)t},\\ e^{-i\Phi_c(t) - ik_\lambda z_0(t)} &= \sum_{n=-\infty}^{\infty}a_n^*(k_\lambda)e^{-i(\Omega_0 + n\Omega_a)t},\\ e^{-i\Phi_c(t) + ik_\lambda z_0(t)} &= \sum_{n=-\infty}^{\infty}a_n^*(-k_\lambda)e^{-i(\Omega_0 + n\Omega_a)t}.\end{aligned} \quad (36)$$

Expanding the exponential terms in Eq. (31) using the above Fourier series results in

$$A_\lambda^{\pm}(\omega) = -\frac{eZ_\lambda v_0}{2}\Bigg[(E_{1\lambda} - iE_{2\lambda})\sum_{n=-\infty}^{\infty} a_n(\mp k_\lambda)\delta(\omega + \Omega_0 + n\Omega_a) + (E_{1\lambda} + iE_{2\lambda})\sum_{n=-\infty}^{\infty} a_n^*(\pm k_\lambda)\delta(\omega - \Omega_0 - n\Omega_a)\Bigg]. \tag{37}$$

E. Frequency comb structure of cyclotron power

Utilizing conventional techniques of handling δ^2 functions and the relationship between the wave number and frequency, the power spectral density for the waveguide mode λ, Eq. (22), is

$$\tilde{P}_\lambda^{\pm}(\omega) = P_{0,\lambda}\sum_{n=-\infty}^{\infty}\left|a_n\left(\pm\frac{\Omega_0 + n\Omega_a}{v_{p,\lambda}}\right)\right|^2 \times \{\delta[\omega - (\Omega_0 + n\Omega_a)] + \delta(\omega + \Omega_0 + n\Omega_a)\}, \tag{38}$$

where $P_{0,\lambda}$ is defined as

$$P_{0,\lambda} = \frac{e^2 v_0^2 Z_\lambda}{8}\left[E_{1\lambda}^2 + E_{2\lambda}^2\right] \tag{39}$$

and $v_{p,\lambda}$ is the phase velocity in the waveguide for the mode λ. Note that there are possible cross terms between the nth positive and the mth negative frequencies when $n + m = -\frac{2\Omega_0}{\Omega_a}$. Because of the small values of a_n for large n, these terms can be neglected.

The measured power spectrum thus exhibits a comb structure in the frequency domain as shown in Fig. 2. For an electron with no axial motion, all the power will be radiated with a frequency Ω_0. An electron with pitch angle other than 90° at the bottom of the trap will undergo axial motion, and as a result some power will be radiated at the harmonic frequencies which are $n\Omega_a$ away from the main peak. Equation (38) indicates that the power in the nth harmonic is

$$P_n = P_{0,\lambda}\left|a_n\left(\pm\frac{\Omega_0 + n\Omega_a}{v_{p,\lambda}}\right)\right|^2. \tag{40}$$

F. Power in particular waveguide geometries

The simplest experimental design choice is a waveguide geometry in which the radiation from the electron will only couple significantly to a single propagating mode. Detailed calculations of $P_{0,\lambda}$ for two interesting examples are included in Appendix B. For the TE_{10} mode in a rectangular waveguide we get

$$P_{0,\mathrm{TE}_{10}} = \frac{Z_{10}e^2 v_0^2}{4wh}\cos^2\left(\frac{\pi x_c}{w}\right), \tag{41}$$

in which Z_{10} is the TE_{10} mode impedance, v_0 is the electron velocity, w and h are the waveguide's width and height, defined to be along x and y directions, respectively, and x_c is the x position of the electron's gyrocenter.

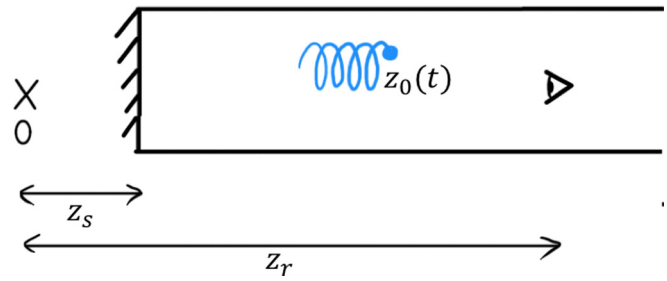

FIG. 3. Schematic of an experiment with an electron undergoing cyclotron motion in a waveguide with a conductive short. The relevant parameters include the origin, O; the position of the electron, z_0; the position of the waveguide short, z_s, on the left side of the waveguide; and the position of the receiver, z_r, on the right side of the waveguide. The magnetic field, B, is parallel to the waveguide axis.

For the TE_{11} mode in a circular waveguide we get

$$P_{0,\mathrm{TE}_{11}} = \frac{Z_{11}e^2 v_0^2}{8\pi\alpha}\left[J_1'^2(k_c\rho_c) + \frac{1}{k_c^2\rho_c^2}J_1^2(k_c\rho_c)\right], \tag{42}$$

in which Z_{11} is the TE_{11} mode impedance, ρ_c defines the radial position of the gyrocenter of the electron in cylindrical coordinates, k_c is the wave number for the cutoff frequency of the mode, and α is defined in Eq. (B8).

IV. EFFECTS OF WAVEGUIDE REFLECTION

In our discussion of waveguides we have assumed infinite length, whereas any experimental realization of a CRES experiment must be finite in length. Allowing that one end of the waveguide must have a receiver, we are left with several options for the treatment of signals at the other end.

One option is to add a second receiver. The signal observed by each receiver is then available for analysis at the cost of supporting two receiver systems. Another option is to install a terminator on one end of the waveguide. The receiver will detect only half of the electron's radiated power and the signal will be the same as the case of the infinite waveguide. The final option, shown in Fig. 3, is to install a conductive short to the end of the waveguide, reflecting signals back to the first receiver. The first two options have been already analyzed. In this section we calculate the effects of the reflector on the power spectral density of the CRES signal.

The total mode excitation at the receiver, $\tilde{B}_\lambda(\omega)$, is a superposition of the direct wave, $\tilde{B}_\lambda^+(\omega)$, and the reflected wave, $\tilde{B}_\lambda^-(\omega)$. The reflection induces a phase shift of 180°. As a consequence, the total mode excitation at the receiver can be written as

$$\begin{aligned}\tilde{B}_\lambda(\omega) &= \tilde{B}_\lambda^+(\omega) + B_\lambda^-(\omega)e^{i\pi} \\ &= B_\lambda^+(\omega) - B_\lambda^-(\omega).\end{aligned} \tag{43}$$

Using the definition of $\tilde{B}_\lambda^{\pm}(\omega)$ given by Eq. (20), we then have

$$\tilde{B}_\lambda(\omega) = A_\lambda^+(\omega)e^{ik_\lambda z_r} - A_\lambda^-(\omega)e^{ik_\lambda(2|z_s - z_t| + z_r)}, \tag{44}$$

where the expression is being evaluated at the receiver's position, z_r, and z_s and z_t are the positions of the reflector and

the trap center respectively. The power spectral density then follows by using Eq. (19),

$$P_\lambda(\omega) = 4P_{0,\lambda} \sum_{n=-\infty}^{\infty} \left| a_n\left(\frac{\Omega_0 + n\Omega_a}{v_{p.\lambda}}\right)\right|^2 \times \cos^2\left[(z_t - z_s)\frac{\Omega_0 + n\Omega_a}{v_{p.\lambda}}\right] \times \{\delta[\omega - (\Omega_0 + n\Omega_a)] + \delta(\omega + \Omega_0 + n\Omega_a)\}. \quad (45)$$

Here we have assumed that the trap is symmetric, in which case $a_n(-k)$ can be written in terms of $a_n(k)$ as in Eq. (A8) (see Appendix A).

This power spectrum still has a comb structure, similarly to the one in the absence of a reflector at the end of the waveguide. However, the amplitude of each peak is now modulated with an extra $\cos^2$ factor, which depends on the distance between the reflector and trap center, $z_t - z_s$. Therefore, while the introduction of a reflector increases the total power collected by the receiver, it also introduces a frequency-dependent amplitude for each peak in the power spectrum.

V. TRAPPING GEOMETRIES

In Sec. III, we built the foundation for calculating the CRES signal's spectral features. From the obtained equations, it is clear that it is impossible to extract a simple analytical solution that is valid and usable for every trap configuration. Therefore, in this section we describe a step-by-step procedure to obtain the spectral properties of a CRES signal. We will then apply this procedure to two simple and useful trap geometries, enabling us to derive numerical solutions for more complicated geometries following these steps:

(i) An appropriate field approximation $B(z)$ must be found. In some cases, where the expression of the exact magnetic field is complex, one can consider using a piecewise approximation of the field.

(ii) With the assumed field profile, the electron's equation of axial motion, Eq. (2), can be solved. Since the effective potential in this equation depends only on the axial position of the electron, we can find a general solution,

$$t = \int_{z_0(0)}^{z_0(t)} \frac{dz'}{\sqrt{\frac{2}{m}[K_e - \mu B(z')]}}. \quad (46)$$

(iii) Once the axial motion of the electron is calculated, the axial frequency follows. For the special case of a symmetric trap, we find

$$\Omega_a^{-1} = \frac{2}{\pi}\int_0^{z_{\max}} \frac{dz}{\sqrt{\frac{2}{m}[E_0 - \mu B(z)]}}. \quad (47)$$

(iv) Once the axial position of the electron is found at any given time, the value of magnetic field experienced by the electron at that time, $B(t)$, follows. Finally, the cyclotron phase, Eq. (27), is found to be

$$\Phi_c(t) = \int_0^t \frac{eB(t')}{\gamma m_e} dt'. \quad (48)$$

(v) To find the power in each peak, the Fourier coefficients introduced in Eq. (34) should be determined by

$$a_n = \frac{1}{T_a}\int_0^{T_a} e^{i[\Phi_c(t) + k_\lambda z(t)]} e^{-i(\Omega_0 + n\Omega_a)t} dt, \quad (49)$$

in which Ω_0 is the average cyclotron frequency given by

$$\Omega_0 = \frac{\Phi_c(T_a)}{T_a}. \quad (50)$$

(vi) The power in each peak of the spectrum can be determined, using Eq. (40), to be

$$P_n = P_{0,\lambda}|a_n|^2. \quad (51)$$

(vii) Finally, the total power radiated by the electron can be calculated by summing over the power of all peaks. This power will define the slopes of tracks in Sec. VI.

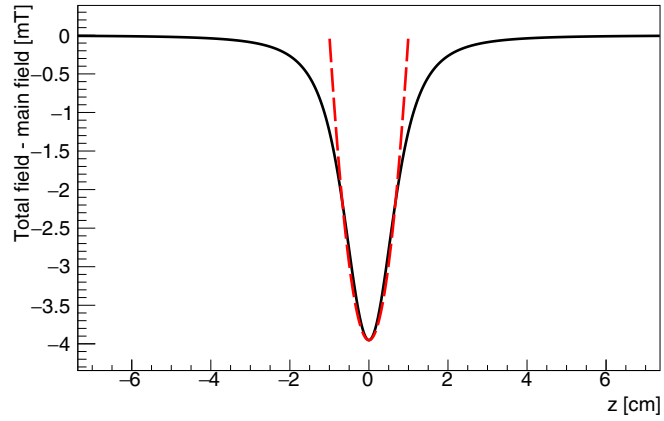

FIG. 4. The on-axis magnetic field profile of a "harmonic" trap (solid black line), generated by a single coil, and the corresponding approximation given by Eq. (52) with $L_0 = 20$ cm (dashed red line).

A. Power spectrum in a "harmonic trap"

The simplest magnetic bottle is realized with a single trapping coil producing a field antiparallel to a background field. This geometry can be approximated as a purely axial field with parabolic z dependence as represented by Fig. 4. It can be described by

$$B_z(z) = B_0\left(1 + \frac{z^2}{L_0^2}\right), \quad (52)$$

in which L_0 is the characteristic length of the trap. Note that this approximation is accurate for trapped electrons with large pitch-angle values that cannot travel to high field regions.

For the harmonic field approximation, electrons undergo simple harmonic motion in the axial direction,

$$z(t) = z_{\max}\sin(\Omega_a t), \quad (53)$$

in which the axial frequency is determined by the axial velocity at the trap minimum,

$$\Omega_a = \frac{v_0 \sin\theta_{\rm bot}}{L_0}, \tag{54}$$

and the maximum displacement for the electron is $z_{\rm max} = L_0 \cot\theta_{\rm bot}$.

The magnetic field seen by the electron as a function of time is

$$B_z(t) = B_0\left[1 + \frac{z_{\rm max}^2}{2L_0^2} - \frac{z_{\rm max}^2}{2L_0^2}\cos(2\Omega_a t)\right]. \tag{55}$$

The cyclotron frequency Eq. (1) of a trapped electron,

$$\Omega_c(t) = \frac{eB_0}{\gamma m_e}\left[1 + \frac{z_{\rm max}^2}{2L_0^2} - \frac{z_{\rm max}^2}{2L_0^2}\cos(2\Omega_a t)\right], \tag{56}$$

follows. The last term describes the modulation in frequency and the first two terms determine the average cyclotron frequency

$$\Omega_0 = \frac{eB_0}{\gamma m_e}\left(1 + \frac{z_{\rm max}^2}{2L_0^2}\right). \tag{57}$$

The cyclotron phase, which can then be found by integrating over the cyclotron frequency, is

$$\Phi_c(t) = \Omega_0 t + q\sin(2\Omega_a t), \tag{58}$$

in which the magnitude of the modulation is

$$q = -\frac{eB_0}{\gamma m_e}\frac{z_{\rm max}^2}{4L_0^2\Omega_a}. \tag{59}$$

To find the power spectrum of the electron's radiation, Fourier coefficients in Eq. (35) are needed and can be calculated using the Jacobi-Anger expansion given by

$$\begin{aligned} e^{i\Phi_c(t)+ik_\lambda z_0(t)} &= e^{i[\Omega_0 t + q\sin(2\Omega_a t) + k_\lambda z_{\rm max}\sin(\Omega_a t)]} \\ &= \sum_{m,p=-\infty}^{\infty} J_m(q)J_p(k_\lambda z_{\rm max})e^{i[\Omega_0+(2m+p)\Omega_a]t}, \end{aligned} \tag{60}$$

where J_n is the nth Bessel function of the first kind. Therefore, the power for each harmonic can be found from Eq. (51) by squaring

$$a_n(k_\lambda) = \sum_{m=-\infty}^{\infty} J_m(q)J_{n-2m}(k_\lambda z_{\rm max}) \tag{61}$$

and using the appropriate $P_{0,\lambda}$ as found in Sec. III F. Let us note that these coefficients, a_n, correspond to the coefficients α_m and β_m defined by Eq. (32) and Eq. (33). This result matches well with our original intuition because the modulation is harmonic, with a modulation index of q for the magnetic field-induced modulation, and a modulation index of $k_\lambda z_{\rm max}$ for the Doppler shift-induced modulation. The relative magnitude of the main peak and sideband powers for typical parameters are shown in Fig. 5.

From Eq. (4), a 4-mT deep trap in a 1-T background magnetic field can trap electrons with pitch angles as small as 86°. In this case, the magnitude of the modulation of the magnetic field experienced by the electron, q, will be smaller than 0.6, while the Doppler effect's modulation, $k_\lambda z_{\rm max}$, can be as large as 10.5. Therefore, $J_m(q)$ can be approximated with δ_{m0}. In this case, the power spectrum will be simplified to

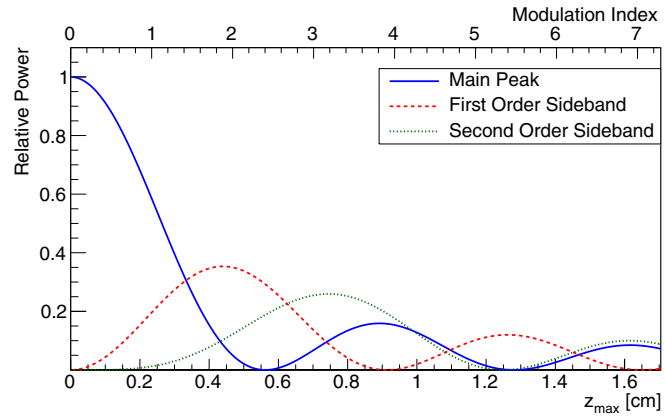

FIG. 5. Relative magnitudes of the sidebands in a harmonic trap as a function of the maximum axial travel, $z_{\rm max}$, of a trapped 30-keV electron. Here we consider an ideal harmonic trap as described in Eq. (52), with a background field of 1 T and an L_0 of 20 cm. No reflection effect is taken into account.

$$\begin{aligned} \tilde{P}_\lambda^{\pm}(\omega) = P_{0,\lambda} &\sum_{n=-\infty}^{\infty} J_n^2(k_\lambda z_{\rm max}) \\ &\times \{\delta[\omega - (\Omega_0 + n\Omega_a)] + \delta(\omega + \Omega_0 + n\Omega_a)\}. \end{aligned} \tag{62}$$

This approximation works well for shallow traps in which $\frac{\Delta B}{B} < 0.002$.

B. Power spectrum in a "bathtub trap"

The harmonic trap described previously has a limited trapping volume. A "bathtub trap," generated using two coils, includes a wide flat region to extend the trapping volume. This field geometry is depicted in Fig. 6. In this case, we approximate the field as a region of constant magnetic field between two half parabolas given piecewise by

$$B_z(z) = \begin{cases} B_0\left[1 + \frac{(z+L_1/2)^2}{L_0^2}\right] & z < -\frac{L_1}{2} \\ B_0 & -\frac{L_1}{2} < z < \frac{L_1}{2} \\ B_0\left[1 + \frac{(z-L_1/2)^2}{L_0^2}\right] & \frac{L_1}{2} < z \end{cases}, \tag{63}$$

in which L_0 is a measure of field gradient in the curved region and L_1 is the width of the flat region.

For convenience, here we define t_0 to be the time when the electron first enters the flat region from the curved region with negative z and we define t_2 to be the time one half-period later when it enters the flat region from the opposite direction. This field configuration results in constant velocity motion when the electron is in the flat region, from $t_0 = 0$ to $t_1 = \frac{L_1}{v_0\cos\theta_{\rm bot}}$, and half harmonic motion at the two ends, for $t_2 - t_1 = \frac{\pi}{\omega_a}$, in which the angular frequency ω_a of the half harmonic motion is defined by $\omega_a = \frac{v_0\sin\theta_{\rm bot}}{L_0}$. The period of axial motion is then $T = 2t_2 = \frac{2\pi}{\Omega_a}$, which means that the frequency of the axial

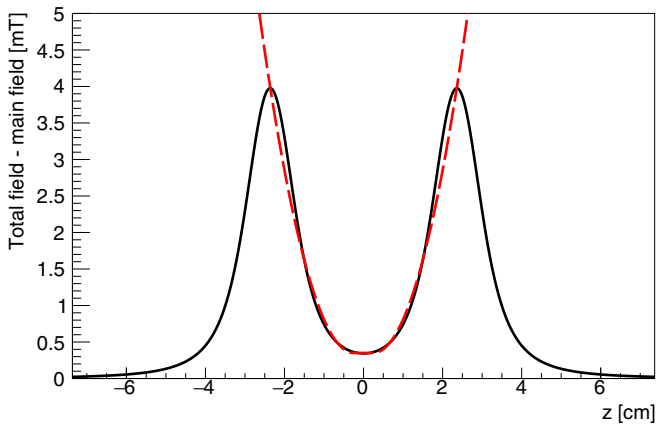

FIG. 6. Magnetic field profile generated by two coils separated by 5 cm, forming a "bathtub" shape (solid black line), and the corresponding approximation given by Eq. (63) with $L_0 = 35$ cm and $L_1 = 0.5$ cm (dashed red line).

motion is

$$\Omega_a = \frac{2\pi}{\frac{2L_1}{v_0\cos\theta_{\rm bot}} + \frac{2\pi L_0}{v_0\sin\theta_{\rm bot}}} = \omega_a\left(1 + \frac{L_1}{\pi L_0}\tan\theta_{\rm bot}\right)^{-1}. \quad (64)$$

The equation of axial motion for an electron is thus

$$z(t) = \begin{cases} v_{z0}t - \frac{L_1}{2} & 0 < t < t_1 \\ z_{\rm max}\sin[\omega_a(t-t_1)] + \frac{L_1}{2} & 0 < t_1 < t < t_2 \\ -v_{z0}(t-t_2) + \frac{L_1}{2} & t_2 < t < t_3 \equiv t_1 + t_2 \\ -z_{\rm max}\sin[\omega_a(t-t_3)] - \frac{L_1}{2} & t_3 < t < T \end{cases}, \quad (65)$$

with $z_{\rm max} = L_0\cot\theta_{\rm bot}$ being the maximum displacement for the electron into the harmonic potential.

Using this equation and magnetic field configuration from Eq. (63), the magnetic field seen by the electron as a function of time is

$$B_z(t) = \begin{cases} B_0 & 0 < t < t_1 \\ B_0\left\{1 + \frac{z_{\rm max}^2}{2L_0^2} - \frac{z_{\rm max}^2}{2L_0^2}\cos[2\omega_a(t-t_1)]\right\} & t_1 < t < t_2 \\ B_0 & t_2 < t < t_3 \\ B_0\left\{1 + \frac{z_{\rm max}^2}{2L_0^2} - \frac{z_{\rm max}^2}{2L_0^2}\cos[2\omega_a(t-t_3)]\right\} & t_3 < t < T \end{cases}. \quad (66)$$

The cyclotron frequency of the electron is therefore

$$\Omega_c(t) = \frac{eB_0}{\gamma m_e}\begin{cases} 1 & 0 < t < t_1 \\ 1 + \frac{z_{\rm max}^2}{2L_0^2} - \frac{z_{\rm max}^2}{2L_0^2}\cos[2\omega_a(t-t_1)] & t_1 < t < t_2 \\ 1 & t_2 < t < t_3 \\ 1 + \frac{z_{\rm max}^2}{2L_0^2} - \frac{z_{\rm max}^2}{2L_0^2}\cos[2\omega_a(t-t_3)] & t_3 < t < T \end{cases}, \quad (67)$$

and the average frequency of cyclotron radiation is

$$\Omega_0 = \frac{eB_0}{\gamma m_e}\left[1 + \frac{z_{\rm max}^2}{2L_0^2}\left(1 + \frac{L_1}{\pi L_0}\tan\theta_{\rm bot}\right)^{-1}\right]. \quad (68)$$

The detailed calculation of the coefficients a_n, which are used to calculate the power, can be found in Appendix C.

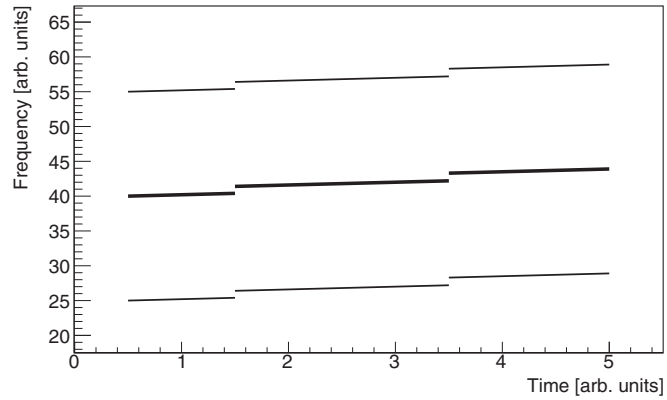

FIG. 7. Schematic of the power (represented by line width), as a function of time and frequency in the absence of a waveguide reflector. The main track and first-order sidebands are shown. Sudden losses of energy (and thus increases of frequency), induced by collisions with background gas particles, happen at 1.5 ms and 3.5 ms.

VI. SPECTRAL FEATURES IN CYCLOTRON RADIATION EMISSION SPECTROSCOPY

In this section we identify the features required for reconstructing the kinematics of an electron in a CRES experiment, based on the relationships in previous sections. We also develop a common terminology for these features.

The power spectrum of the signal generated by an electron possesses a comb structure given by Eq. (38). If we represent the power spectrum as a function of time in a spectrogram, then the excess of power forms connected structures that we call *tracks*. Figure 7 represents the tracks coming from the comb structure of the spectrum. The track at the average cyclotron frequency, given by Eq. (7), is called the *main track*. As the electron radiates energy, the cyclotron frequency increases, causing the tracks to have a positive slope. For any given trap configuration, the track's slope, S, is proportional to the power radiated into both propagating and nonpropagating modes. According to Eq. (7) this relation can be written as

$$S = \frac{\Omega_c}{m_e c^2 + K_0}P. \quad (69)$$

Electrons can scatter off a molecule of the residual gas in the waveguide, causing abrupt energy losses, changes of pitch angle, and breaks in the observed tracks.

The tracks parallel to the main tracks we call *sidebands*. These tracks are located at multiples of the axial frequency, $f_a = \frac{\Omega_a}{2\pi}$, away from the main track; the *order* of a sideband corresponds to this multiplicity. As long as we only consider time intervals short enough that the power radiated does not significantly change the axial frequency, sidebands will appear parallel to the main track. Equations (54) and (64) show how the axial frequency, measured from the frequency distance to sidebands, can be used to relate the pitch angle and kinetic energy of an electron in a harmonic or bathtub traps.

The distribution of power between a main track and its sidebands depends on the electron's energy and pitch angle.

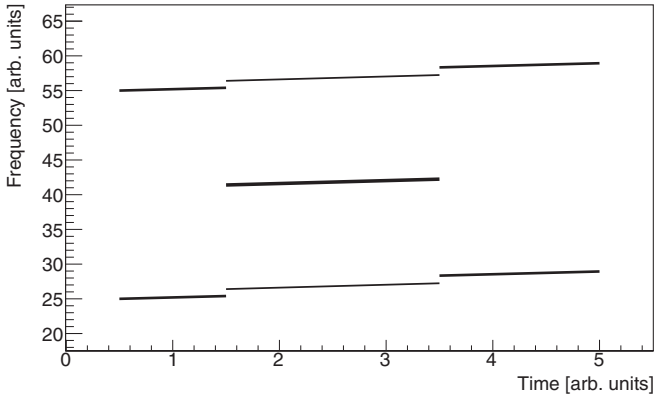

FIG. 8. Schematic of the power (represented by line width) as a function of time and frequency in the presence of a waveguide reflector. The main track appears and disappears as the kinematic parameters (such as the pitch angle) change as a result of collisions with background gas particles.

In the presence of a reflector on one end of the waveguide, as described in Sec. IV, the distance between the trap and the reflector will also impact the power distribution as shown in Fig. 8. In realistic experiments, this is further complicated as tracks with suppressed power will be indistinguishable from noise.

VII. EXTRACTION OF KINEMATIC PARAMETERS FROM A MEASURED SPECTRUM

The previous sections show that the primary observable parameters of a CRES signal are the frequency of the main track, the frequency separating the sidebands, the power in both the main track and sidebands, and the slope of the main track.

For a given configuration of trapping field and waveguide, these parameters are completely determined by the electron's kinetic energy and pitch angle. However, the converse is not in general true. The axial frequency in a real magnetic trap is double valued with respect to the pitch angle whenever the floor of the trap is flatter than harmonic. This is because the axial frequency is relatively low both for small amplitudes and for amplitudes that almost eject the electron over the trap-field maxima, and it reaches a broad maximum for intermediate amplitudes. Other ambiguities arise when resonant structures such as those described in Sec. IV cause the slope to have multiple values. These ambiguities can be mitigated at the design stage and by making use of all the available information in the signal. We will now give a concrete example of predicting the observable parameters from a particular trapping field and then speculate on the observations needed to reconstruct the electron's initial kinetic energy.

For our example in Fig. 9, we will use a bathtub trap with an L_0 of 35 cm and an L_1 of 0.5 cm in a 1.07-cm-wide rectangular waveguide. We consider a short on one end of the waveguide, a distance 0.6 cm away from the trap center, and a 1T background magnetic field. We will examine predicted signals from electrons with 30 keV of kinetic energy and with different pitch angles. We find the power in the nth harmonic

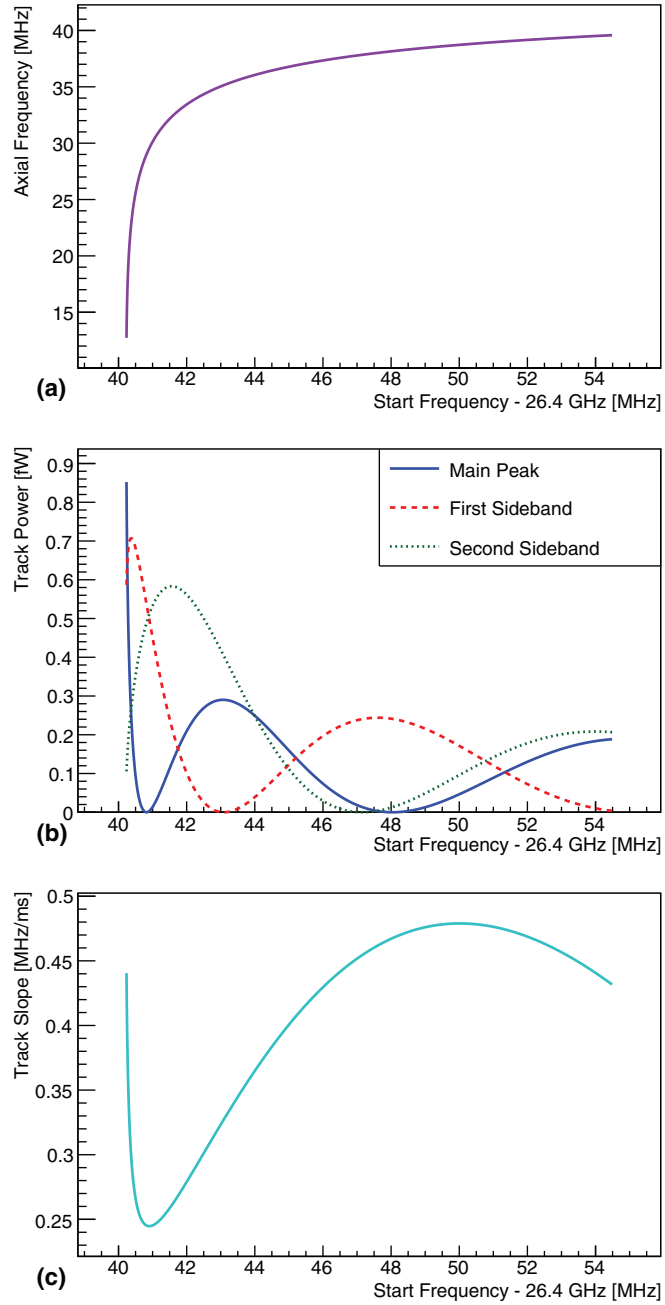

FIG. 9. Spectral features of the CRES signal for 30-keV electrons with different values of pitch angle and single radial position at $\rho = 0$ cm, trapped in an ideal bathtub trap described by Eq. (63) with $L_0 = 35$ cm and $L_1 = 0.5$ cm, in a 1-T background field including the effect of a short. An electron with a pitch angle of 90° has a start frequency of 26.44 GHz while electrons with lower pitch angles are subject to pitch-angle effects which increase their start frequencies. This shift can systematically affect energy measurements in CRES experiments. The above plots illustrate how different measurable quantities in a CRES experiment can be used to correct for this frequency shift.

for this situation using Eq. (45), which includes the short, using the power from Eq. (41), which is for the rectangular waveguide. The Fourier coefficients for the bathtub trap are

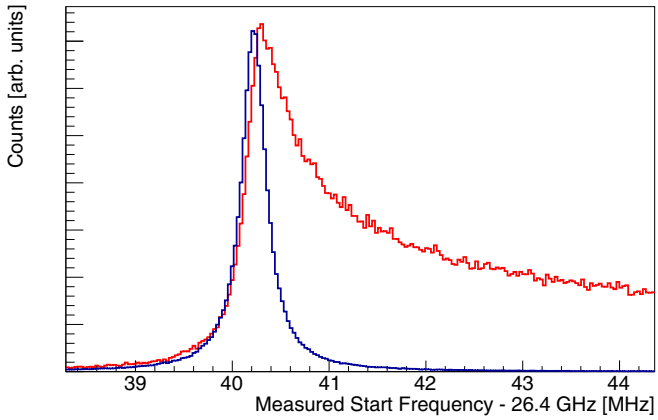

FIG. 10. Simulation of the energy spectrum of electrons sampled from a 60-eV wide Lorentzian, centered at 30 keV, in a 1-T background magnetic field. In blue (light gray in black and white print), the spectrum of the extracted start frequencies for an idealized case where the magnetic field is flat and all electrons have a 90° pitch angle. In red (dark gray in black and white print), the actual line shape when the electrons have an isotropic momentum distribution and are confined in a 4-mT deep ideal harmonic trap as given in Eq. (52). The blue histogram is scaled down, so it can be compared with the red one.

found in Appendix C. Therefore we have

$$P_\lambda(\omega) = \frac{Z_{10}e^2v_0^2}{\pi wh}\cos^2\left(\frac{\pi x_c}{w}\right) \times \sum_{n=-\infty}^{\infty} |a_n(k_\lambda)|^2 \cos^2\left[(z_t - z_s)k_\lambda\right] \times \{\delta[\omega - (\Omega_0 + n\Omega_a)] + \delta(\omega + \Omega_0 + n\Omega_a)\}. \quad (70)$$

Of the observables, the *start frequency* of the main track is the most strongly related to the electron's kinetic energy. The cyclotron frequency of a 30-keV electron, with a pitch angle of 90° at the center of the trap, is 26.44 GHz. However, this frequency is increased by the electron's pitch angle as described in Sec. II D. The distortion of the distribution of main track frequencies by pitch angle is shown in Fig. 10.

The other signal parameters can be used to correct for the pitch-angle effect and recover the true kinetic energy of the electron. Decreasing the pitch angle will simultaneously increase the start frequency and effects the other parameters discussed above. In principle, only a subset of the parameters are needed to find the pitch angle and recover the correct energy.

A sufficiently precise measurement of the axial frequency alone can be used to correct the main track frequency, yielding the cyclotron frequency at the center of the trap. However, extraction of the axial frequency is possible only for pitch angles for which there are at least two visible tracks above the noise level.

In other cases, other parameters must be used. Track power carries valuable information, though typically power measurements in CRES experiments are less precise than frequency measurements and may not be possible if the noise level is high. Furthermore, the power is double valued for nonshallow trap geometries that can trap electrons with smaller pitch angles. Determining a track's slope is a frequency measurement, measurable even if the main track or sidebands are absent, and therefore is a most reliable parameter for correction. However, the slope is double valued for this example. The precise algorithm for combining the parameters to achieve a high-resolution energy measurement will, therefore, depend on the particular geometry and signal-to-noise of the CRES experiment.

VIII. CONCLUSION

We have found that electrons in a CRES experiment undergo nontrivial but predictable motion within a magnetic bottle, and this motion affects the detected cyclotron signal. We identified the carrier and sideband structure of the signal and have shown that these features encode the entirety of the electron's kinematic parameters. Following the results derived here, a sufficiently precise measurement of these features should allow complete reconstruction of the electron's kinetic energy, which is necessary for proposed CRES experiments to achieve their desired sensitivity. In fact, the measurable features overconstrain the kinematic parameters and may be able to calibrate some of the detector configuration as well. Notably, we point out that for configurations where the electron undergoes axial motion larger than a half wavelength of cyclotron radiation, the modulation is such that detection and interpretation of sidebands is necessary to detect all trapped electrons.

The results here should be directly useful in improving the energy resolution of β-decay energies measured with the CRES technique. The practicalities of signal detection and reconstruction will depend on the particular apparatus design and detection scheme, in particular the signal-to-noise ratio of the sidebands, and we leave a discussion of the precise reconstruction algorithm and ultimate resolution to future work.

ACKNOWLEDGMENTS

This material is based upon work supported by the following sources: the U.S. Department of Energy Office of Science, Office of Nuclear Physics, under Award No. DE SC0014130 to University of California Santa Barbara (UCSB), under Award No. DE-SC0011091 to Massachusetts Institute of Technology (MIT), under the Early Career Research Program to Pacific Northwest National Laboratory (PNNL), a multiprogram national laboratory operated by Battelle for the U.S. Department of Energy under Contract No. DE-AC05-76RL01830, under Award No. DE-FG02-97ER41020 to the University of Washington (UW), and under Award No. DE-SC0012654 to Yale University; the National Science Foundation under Awards No. 1205100 and No. 1505678 to MIT; Laboratory Directed Research and Development (LDRD) at Lawrence Livermore National Laboratory (LLNL) (18-ERD-028), prepared by LLNL under Contract DE-AC52-07NA27344; the MIT Wade Fellowship; the LDRD Program

at PNNL; the UW Royalty Research Foundation. A portion of the research was performed using Research Computing at PNNL. We further acknowledge support from Yale University, the PRISMA Cluster of Excellence at the University of Mainz, and the Karlsruhe Institute of Technology (KIT) Center Elementary Particle and Astroparticle Physics (KCETA).

APPENDIX A: PROPERTY OF THE FOURIER COEFFICIENTS IN A SYMMETRIC TRAP

In a trap where the magnetic field distortion is symmetric with respect to the center of the trap, we expect the same amplitude of radiation to propagate in both directions in the waveguide. This means that we need to show that

$$|a_n(-k_\lambda)|^2 = |a_n(k_\lambda)|^2. \tag{A1}$$

Two useful expressions in symmetric traps will assist us in deriving this relation. The first relates to the periodicity of the electron's position, z_0, in a symmetric trap, given by

$$-[z_0(t) - z_t] = z_0\left(t + \frac{T_a}{2}\right) - z_t, \tag{A2}$$

in which z_t is the axial position of the center of the trap. Furthermore, a symmetric trap forces the cyclotron frequency to be periodic, with period equal to half of the axial motion's period. Therefore the cyclotron phase satisfies

$$\Phi_c\left(t + \frac{T_a}{2}\right) = \Omega_0\frac{T_a}{2} + \Phi_c(t). \tag{A3}$$

Utilizing Eq. (A2) for $\Phi_c(t)$ and Eq. (A3) to rewrite $k_\lambda z_0(t)$, we can write

$$\begin{aligned}\Phi_c(t) - k_\lambda z_0(t) = \Phi_c\left(t + \frac{T_a}{2}\right) - \Omega_0\frac{T_a}{2} \\ + k_\lambda z_0\left(t + \frac{T_a}{2}\right) - 2k_\lambda z_t.\end{aligned} \tag{A4}$$

Therefore we have

$$e^{i\Phi_c(t) - ik_\lambda z_0(t)} = e^{-i\Omega_0\frac{T_a}{2} - 2ik_\lambda z_t} e^{i\Phi_c(t+\frac{T_a}{2}) + ik_\lambda z_0(t+\frac{T_a}{2})}. \tag{A5}$$

Using Eq. (34), we expand the second exponent to get

$$\begin{aligned}e^{i\Phi_c(t) - ik_\lambda z_0(t)} &= e^{-2ik_\lambda z_t - i\Omega_0\frac{T_a}{2}} \sum_{n=-\infty}^{\infty} a_n(k_\lambda) e^{i(\Omega_0 + n\Omega_a)(t+\frac{T_a}{2})} \\ &= e^{-2ik_\lambda z_t} \sum_{n=-\infty}^{\infty} (-1)^n a_n(k_\lambda) e^{i(\Omega_0 + n\Omega_a)t}.\end{aligned} \tag{A6}$$

By equating the coefficients with those of the first expression in Eq. (36), we arrive at the form

$$a_n(-k_\lambda) = (-1)^n e^{-2ik_\lambda z_t} a_n(k_\lambda), \tag{A7}$$

which is consistent with our expectation of equal power propagating in both directions, since

$$|a_n(-k_\lambda)|^2 = |a_n(k_\lambda)|^2. \tag{A8}$$

APPENDIX B: $P_{0,\lambda}$ CALCULATION FOR TWO SPECIFIC WAVEGUIDE GEOMETRIES

The power amplitude, $P_{0,\lambda}$, was introduced in Eq. (39) as a measurement of an electron's coupling to a waveguide mode. The calculation details for two particularly relevant cases are shown here.

1. Rectangular waveguide TE_{10} mode

The first example is the fundamental mode of a rectangular waveguide. For such a waveguide, with w being its longer dimension (defined to be along the x axis) and h the smaller one (along the y axis), the electric field has the form

$$E_y(x) = K\cos\left(\frac{\pi x}{w}\right)\hat{y}. \tag{B1}$$

Equation (15) can now be used to find the normalization factor, giving

$$\int_{\mathcal{A}} K^2\cos^2\left(\frac{\pi x}{w}\right)dxdy = 1 \Rightarrow K = \sqrt{\frac{2}{wh}}. \tag{B2}$$

With the normalized field, the expression for $P_{0,\mathrm{TE10}}$ follows from the definition in Eq. (39) and is found to be

$$\begin{aligned}P_{0,\mathrm{TE}_{10}} &= \frac{Z_{10}e^2v_0^2}{8}\left[\sqrt{\frac{2}{wh}}\cos\left(\frac{\pi x_c}{w}\right)\right]^2 \\ &= \frac{Z_{10}e^2v_0^2}{4wh}\cos^2\left(\frac{\pi x_c}{w}\right).\end{aligned} \tag{B3}$$

2. Circular waveguide TE_{11} mode

The second example to consider is that of a circular waveguide with radius R. The TE_{11} mode has the lowest cutoff frequency in a circular waveguide and the associated wave number is $k_c = \frac{1.841}{R}$. This mode consists of two degenerate modes for which the electric field can be found in Ref. [17],

$$\begin{aligned}E_{1\rho}(\rho,\phi) &= K\frac{-i\omega\mu}{k_c^2\rho}\cos(\phi)J_1(k_c\rho), \\ E_{1\phi}(\rho,\phi) &= K\frac{i\omega\mu}{k_c}\sin(\phi)J_1'(k_c\rho), \\ E_{1z}(\rho,\phi) &= 0\end{aligned} \tag{B4}$$

and

$$\begin{aligned}E_{2\rho}(\rho,\phi) &= K'\frac{-i\omega\mu}{k_c^2\rho}\sin(\phi)J_1(k_c\rho), \\ E_{2\phi}(\rho,\phi) &= K'\frac{i\omega\mu}{k_c}\cos(\phi)J_1'(k_c\rho), \\ E_{2z}(\rho,\phi) &= 0.\end{aligned} \tag{B5}$$

The same technique is used to find the normalized fields,

$$\begin{aligned}1 &= \int_{\mathcal{A}}\left[E_{1\rho}^2(\rho,\phi) + E_{1\phi}^2(\rho,\phi)\right]\rho d\rho d\phi \\ &= -K^2\pi\frac{\omega^2\mu^2}{2k_c^2}\int_0^R\left[\frac{J_1^2(k_c\rho)}{k_c^2\rho^2} + J_1'^2(k_c\rho)\right]\rho d\rho.\end{aligned} \tag{B6}$$

Hence the normalization factor can be found to be

$$K = K' = \frac{ik_c}{\omega\mu\sqrt{\pi\alpha}} \tag{B7}$$

in which

$$\alpha = \int_0^R \left[\frac{J_1^2(k_c\rho)}{k_c^2\rho^2} + J_1'^2(k_c\rho)\right]\rho d\rho. \tag{B8}$$

The calculation of the coefficients $P_{0,\mathrm{TE}_{11}}$ follows the rectangular waveguide calculation with one difference. That is, to find the power in the waveguide, the two degenerate modes' powers should be added together. This gives us

$$\begin{aligned} P_{0,\mathrm{TE}_{11}} &= \frac{Z_{11}e^2v_0^2}{8}\left[E_{1\phi}^2 + E_{1\rho}^2 + E_{2\phi}^2 + E_{2\rho}^2\right] \\ &= \frac{Z_{11}e^2v_0^2}{8\pi\alpha}\left[J_1'^2(k_c\rho_c) + \frac{1}{k_c^2\rho_c^2}J_1^2(k_c\rho_c)\right]. \end{aligned} \tag{B9}$$

APPENDIX C: BATHTUB TRAP CALCULATION

The "bathtub" trapping geometry was introduced in Sec. V. Here we present detailed calculations of both the phase and the axial motion Fourier expansion coefficients, defined by Eq. (32) and Eq. (33), respectively.

First, we define the frequency difference between the average cyclotron and the frequency at the bottom of the trap using Eq. (64),

$$\begin{aligned} \Delta\Omega \equiv \Omega_0 - \frac{eB_0}{\gamma m_e} &= \frac{\Omega_c}{2}\frac{z_{\max}^2}{L_0^2}\left(1 + \frac{L_1}{\pi L_0}\tan\theta\right)^{-1} \\ &= \frac{\Omega_c}{2}\frac{z_{\max}^2}{L_0^2}\frac{\Omega_a}{\omega_a}. \end{aligned} \tag{C1}$$

The perturbation to the average cyclotron phase can be written as

$$\Phi_c(t) - \Omega_0 t = \begin{cases} -\Delta\Omega t & 0 < t < t_1 \\ \Delta\Omega\frac{\omega_a}{\Omega_a}(t-t_1) - \frac{\Delta\Omega}{2\Omega_a}\sin[2\omega_a(t-t_1)] - \Delta\Omega t & t_1 < t < t_2 \\ -\Delta\Omega(t-t_2) & t_2 < t < t_3 \\ \Delta\Omega\frac{\omega_a}{\Omega_a}(t-t_3) - \frac{\Delta\Omega}{2\Omega_a}\sin[2\omega_a(t-t_3)] - \Delta\Omega(t-t_2) & t_3 < t < T \end{cases}. \tag{C2}$$

The coefficients, α_n, can then be found to be

$$\alpha_n = \frac{1}{T}\int_0^T e^{i\Phi_c(t) - i\Omega_0 t}e^{-in\Omega_a t}dt. \tag{C3}$$

The integral can be computed by splitting it into four pieces as

$$\alpha_n = \frac{1}{T}(A_n + B_n + C_n + D_n), \tag{C4}$$

in which

$$\begin{aligned} A_n &= \int_0^{t_1} e^{i\Phi_c(t) - i\Omega_0 t}e^{-in\Omega_a t}dt \\ &= t_1 e^{-i(\Delta\Omega + n\Omega_a)\frac{t_1}{2}}\,\mathrm{sinc}\left[(\Delta\Omega + n\Omega_a)\frac{t_1}{2}\right], \end{aligned} \tag{C5}$$

$$\begin{aligned} B_n &= \int_{t_1}^{t_2} e^{i\Phi_c(t) - i\Omega_0 t}e^{-in\Omega_a t}dt \\ &= \frac{\pi}{\omega_a}e^{-i(\Delta\Omega + n\Omega_a)t_1/2}\sum_{m=-\infty}^{\infty} J_m\left(\frac{\Delta\Omega}{2\Omega_a}\right)e^{-in\frac{\pi}{2}} \\ &\quad \times \mathrm{sinc}\left(\Delta\Omega\frac{t_1}{2} - \frac{n\pi}{2}\frac{\Omega_a}{\omega_a} + m\pi\right), \end{aligned} \tag{C6}$$

$$C_n = \int_{t_2}^{t_3} e^{i\Phi_c(t) - i\Omega_0 t}e^{-in\Omega_a t}dt = (-1)^n A_n, \tag{C7}$$

$$D_n = \int_{t_3}^{T} e^{i\Phi_c(t) - i\Omega_0 t}e^{-in\Omega_a t}dt = (-1)^n B_n. \tag{C8}$$

Note that for odd values of n the coefficient α_n is zero.

The determination of β_n follows in a similar manner. The electron's equation of motion [Eq. (65)] gives

$$\beta_n = \frac{1}{T}\int_0^T e^{ik_\lambda z(t)}e^{-in\Omega_a t}dt = \frac{1}{T}(E_n + F_n + G_n + H_n), \tag{C9}$$

where

$$\begin{aligned} E_n &= \int_0^{t_1} e^{ik_\lambda z(t)}e^{-in\Omega_a t}dt \\ &= t_1 e^{-in\Omega_a\frac{t_1}{2}}\,\mathrm{sinc}\left[(k_\lambda v_{z0} - n\Omega_a)\frac{t_1}{2}\right], \end{aligned} \tag{C10}$$

$$\begin{aligned} F_n &= \int_{t_1}^{t_2} e^{ik_\lambda z(t)}e^{-in\Omega_a t}dt \\ &= e^{ik_\lambda L_1/2}\frac{\pi}{\omega_a}e^{-in\Omega_a t1/2} \\ &\quad \times \sum_{m=-\infty}^{\infty} J_m(k_\lambda z_{\max})i^{m-n}\mathrm{sinc}\left(\frac{m\pi}{2} - \frac{n\pi}{2}\frac{\Omega_a}{\omega_a}\right), \end{aligned} \tag{C11}$$

$$\begin{aligned} G_n &= \int_{t_2}^{t_3} e^{ik_\lambda z(t)}e^{-in\Omega_a t}dt \\ &= (-1)^n t_1 e^{-in\Omega_a\frac{t_1}{2}}\,\mathrm{sinc}\left[(k_\lambda v_{z0} + n\Omega_a)\frac{t_1}{2}\right], \end{aligned} \tag{C12}$$

$$\begin{aligned} H_n &= \int_{t_3}^{T} e^{ik_\lambda z(t)}e^{-in\Omega_a t}dt \\ &= (-1)^n e^{-ik_\lambda L_1/2}\frac{\pi}{\omega_a}e^{-in\Omega_a t1/2} \\ &\quad \times \sum_{m=-\infty}^{\infty} J_m(k_\lambda z_{\max})i^{-m-n}\mathrm{sinc}\left(\frac{m\pi}{2} - \frac{n\pi}{2}\frac{\Omega_a}{\omega_a}\right). \end{aligned} \tag{C13}$$

The coefficients α_n and β_n can be used to find a_n as defined in Eq. (35). These a_n coefficients are a measure of the relative power in the nth peak of the power spectrum, according to Eq. (38).

[1] F. Penning, Physica **3**, 873 (1936).

[2] R. Van Dyck, Jr., P. Schwinberg, and H. Dehmelt, in *Atomic Physics 9*, edited by R. Van Dyck, Jr. and E. Forston (World Scientific, Singapore, 1984), p. 83.

[3] D. Hanneke, S. Fogwell, and G. Gabrielse, Phys. Rev. Lett. **100**, 120801 (2008).

[4] L. S. Brown and G. Gabrielse, Rev. Mod. Phys. **58**, 233 (1986).

[5] B. Monreal and J. A. Formaggio, Phys. Rev. D **80**, 051301(R) (2009).

[6] D. M. Asner, R. F. Bradley, L. de Viveiros, P. J. Doe, J. L. Fernandes, M. Fertl, E. C. Finn, J. A. Formaggio, D. Furse, A. M. Jones, J. N. Kofron, B. H. LaRoque, M. Leber, E. L. McBride, M. L. Miller, P. Mohanmurthy, B. Monreal, N. S. Oblath, R. G. H. Robertson, L. Rosenberg, G. Rybka, D. Rysewyk, M. G. Sternberg, J. R. Tedeschi, T. Thummler, B. A. VanDevender, and N. L. Woods (Project 8 Collaboration), Phys. Rev. Lett. **114**, 162501 (2015).

[7] A. Ashtari Esfahani, D. Asner, S. Böser, R. Cervantes, C. Claessens, P. Doe, S. Doeleman, J. Fernandez, M. Fertl, E. Finn, J. Formaggio, D. Furse, M. Guigue, K. Heeger, A. M. Jones, K. Kazkaz, J. Kofron, C. Lamb, B. LaRoque, E. Machado, E. McBride, M. Miller, B. Monreal, P. Mohanmurthy, J. Nikkel, N. Oblath, W. Pettus, H. Robertson, L. Rosenberg, G. Rybka, D. Rysewyk, L. Saldaña, P. Slocum, M. Sternberg, J. Tedeschi, T. Thuemmler, B. VanDevender, L. Vertatschitsch, L. de Viveiros, M. Wachtendonk, J. Weintroub, N. Woods, A. Young, and E. Zayas, J. Phys. G: Nucl. Part. Phys. **44**, 5 (2017).

[8] E. W. Otten and C. Weinheimer, Rep. Prog. Phys. **71**, 086201 (2008).

[9] K. P. Hickerson, X. Sun, Y. Bagdasarova, D. Bravo-Berguno, L. J. Broussard, M. A.-P. Brown, R. Carr, S. Currie, X. Ding, B. W. Filippone, A. Garcia, P. Geltenbort, J. Hoagland, A. T. Holley, R. Hong, T. M. Ito, A. Knecht, C. Y. Liu, J. L. Liu, M. Makela, R. R. Mammei, J. W. Martin, D. Melconian, M. P. Mendenhall, S. D. Moore, C. L. Morris, R. W. Pattie, A. PerezGalvan, R. Picker, M. L. Pitt, B. Plaster, J. C. Ramsey, R. Rios, A. Saunders, S. J. Seestrom, E. I. Sharapov, W. E. Sondheim, E. Tatar, R. B. Vogelaar, B. Vorn Dick, C. Wrede, A. R. Young, and B. A. Zeck (UCNA Collaboration), Phys. Rev. C **96**, 042501(R) (2017).

[10] D. Počanić, R. Alarcon, L. Alonzi, S. Baeßler, S. Balascuta, J. Bowman, M. Bychkov, J. Byrne, J. Calarco, V. Cianciolo, C. Crawford, E. Frlež, M. Gericke, G. Greene, R. Grzywacz, V. Gudkov, F. Hersman, A. Klein, J. Martin, S. Page, A. Palladino, S. Penttilä, K. Rykaczewski, W. Wilburn, A. Young, and G. Young, Nucl. Instrum. Methods A **611**, 211 (2009).

[11] H. Dehmelt and P. Ekstrom, Bull. Am. Phys. Soc. **18**, 727 (1973).

[12] T. Sekhar, *Communication Theory*, Electrical and Electronic Series (Tata McGraw-Hill, New York, 2005).

[13] T. G. Northrop, *The Adiabatic Motion of Particles* (Interscience Publishers, New York, 1963).

[14] R. Fitzpatrick, *Introduction to Plasma Physics* (CRC Press, Boca Raton, FL, 2014).

[15] J. D. Jackson, *Classical Electrodynamics*, 3rd ed. (Wiley, New York, 1999).

[16] R. Collin, IEEE Trans. Microwave Theory Tech. **13**, 413 (1965).

[17] D. Pozar, *Microwave Engineering* (Wiley, New York, 2004).